JOURNAL OF MOLECULAR SPECTROSCOPY 92, 391–409 (1982)

Fourier Transform Spectroscopy of VO: Rotational Structure in the $A^4\Pi$–$X^4\Sigma^-$ System Near 10 500 Å

A. S-C. CHEUNG, A.W. TAYLOR, AND A. J. MERER

Department of Chemistry, University of British Columbia, 2036 Main Mall, Vancouver, B. C., V6T 1Y6, Canada

The $A^4\Pi$–$X^4\Sigma^-$ electronic transition of VO in the near infrared was recorded at Doppler-limited resolution by Fourier transform spectroscopy, and rotational analyses performed for the (0, 0) band at 1.05 μm and the (0, 1) band at 1.18 μm. The $A^4\Pi$ state is found to have comparatively small spin–orbit coupling (A = 35.19 cm^{-1}) so that is is almost completely uncoupled to case (b) at the highest N values observed, near N = 90. The hyperfine structure due to the ^{51}V nucleus (I = 7/2) is prominent in the $^4\Pi_{5/2}$–$X^4\Sigma^-$ subband, and in many of the spin satellite branches; at high N values, where only main branches ($\Delta N = \Delta J$) occur, the lines are sharp, indicating that the hyperfine b parameter (the coefficient of $\mathbf{I}\cdot\mathbf{S}$ in the magnetic hyperfine Hamiltonian) is the same in the $A^4\Pi$ and $X^4\Sigma^-$ states. The electron configuration of the $A^4\Pi$ state is therefore $(4s\sigma)^1(3d\delta)^1(4p\pi)^1$.

1. INTRODUCTION

Vanadium monoxide, VO, is present in considerable amounts in the atmospheres of cool stars, to the extent that its two electronic band systems in the near infrared are used for the spectral classification of stars of types M7–M9 (*1*). Both of these systems, A–X near 10 500 Å and $B^4\Pi$–$X^4\Sigma^-$ near 7900 Å, were in fact first found in stellar spectra (*2*, *3*) before laboratory work, respectively by Lagerqvist and Selin (*4*) and Keenan and Schroeder (*5*), proved that VO is the carrier. The purpose of this paper is to report rotational analyses of the (0, 0) and (0, 1) bands of the A–X system from high-dispersion Fourier transform emission spectra; the A–X system is shown to be another $^4\Pi$–$^4\Sigma^-$ transition.

The $A^4\Pi$ state of VO is found to have quite small spin–orbit coupling, so that the rotational and hyperfine structure follows case (a_β) coupling at low rotational quantum numbers, but is almost totally uncoupled to case ($b_{\beta J}$) coupling at the highest observed quantum numbers. The hyperfine structure caused by the ^{51}V nucleus (I = 7/2) is not resolved in the spectra reported here, but an interesting result is that the hyperfine parameter b for the $A^4\Pi$ state can be estimated from the lineshapes at high N values and is found to be essentially the same as in the ground $X^4\Sigma^-$ state. The conclusion is that the $A^4\Pi$ state comes from an electron configuration containing an unpaired $4s\sigma$ electron, as does the ground state.

In contrast to the other excited states of VO the $A^4\Pi$, v = 0 level is unperturbed rotationally; it therefore provides one of the very few examples known where the energy formulas for $^4\Pi$ states can be checked directly against observation.

0022-2852/82/040391-19$02.00/0

2. EXPERIMENTAL DETAILS

The near infrared electronic transitions of VO in the region 6000–14 000 cm^{-1} were recorded in emission using the 1-m Fourier transform spectrometer constructed by Dr. J. W. Brault for the McMath Solar Telescope at Kitt Peak National Observatory, Tucson, Arizona.[1] The source was a microwave discharge through flowing $VOCl_3$ and helium at low pressures, which was focused directly into the aperture of the spectrometer. An indium antimonide detector cooled by liquid nitrogen was used, and the resolving power of the spectrometer was set to approximately 800 000. Forty-two interferograms, each taking 6 min to record, were coadded for the final transform. The resulting spectrum, consisting of tables of emission intensity against wavenumber for every 0.013608 cm^{-1}, was processed by a third-degree polynomial fitting program to extract the positions of the line peaks.

3. APPEARANCE OF THE SPECTRUM

The spectrum of VO in the near infrared down to 6000 cm^{-1} consists of the two electronic transitions $B\,^4\Pi$–$X\,^4\Sigma^-$ and $A\,^4\Pi$–$X\,^4\Sigma^-$. The B–X system is very much stronger than the A–X system under our discharge conditions, so that the B–X progressions and sequences mask most of the A–X system except for the (0, 0) and (0, 1) bands. Even the (0, 0) band of the A–X system (which is by far the strongest band) is not free from overlapping B–X structure, which causes some difficulty in the analysis. The main heads of the A–X (0, 0) band are illustrated in Fig. 1; each of the four subbands produces one strong head ($^SR_{43}$, R_3, $^RQ_{21}$, and R_1), and there is also a less prominent Q_1 head in the $^4\Pi_{-1/2}$–$^4\Sigma^-$ subband. Two other heads, belonging to the B–X (1, 4) band, appear in the region of the $^4\Pi_{5/2}$–$^4\Sigma^-$ subband; they have not been identified in the figure, though their branch structure is readily picked out at higher dispersion.

The A–X (0, 1) band is qualitatively similar, though since it is weaker the background of B–X lines is more troublesome. The A–X (1, 0) band is so heavily overlapped by B–X structure that we have not been able to analyze it; the $^SR_{43}$ head appears to be at 10 503.3 cm^{-1} but even this is not definite.

4. ENERGY LEVELS OF $^4\Pi$ AND $^4\Sigma$ STATES

Energy levels for $^4\Pi$ electronic states have been considered by a number of authors (*6–11*). The most detailed treatment is that of Fémènias (*9*), who has given a full explanation of how to calculate the matrix elements for the higher-order centrifugal distortion terms. Detailed analyses of $^4\Pi$ states, against which to test the formulas, are less common; the best examples come from the spectra of O_2^+ (*10*) and NO (*12*).

$^4\Sigma$ states, on the other hand, are much more numerous, and have been extensively treated (*6, 7, 9, 10, 13–17*). It will therefore only be necessary to sketch the Hamiltonian and its derivation, and to give the matrices we have used.

Following van Vleck (*18*) we take the rotational Hamiltonian, the first- and

[1] Kitt Peak National Observatory is operated by the Association of Universities for Research in Astronomy under contract with the National Science Foundation of the United States.

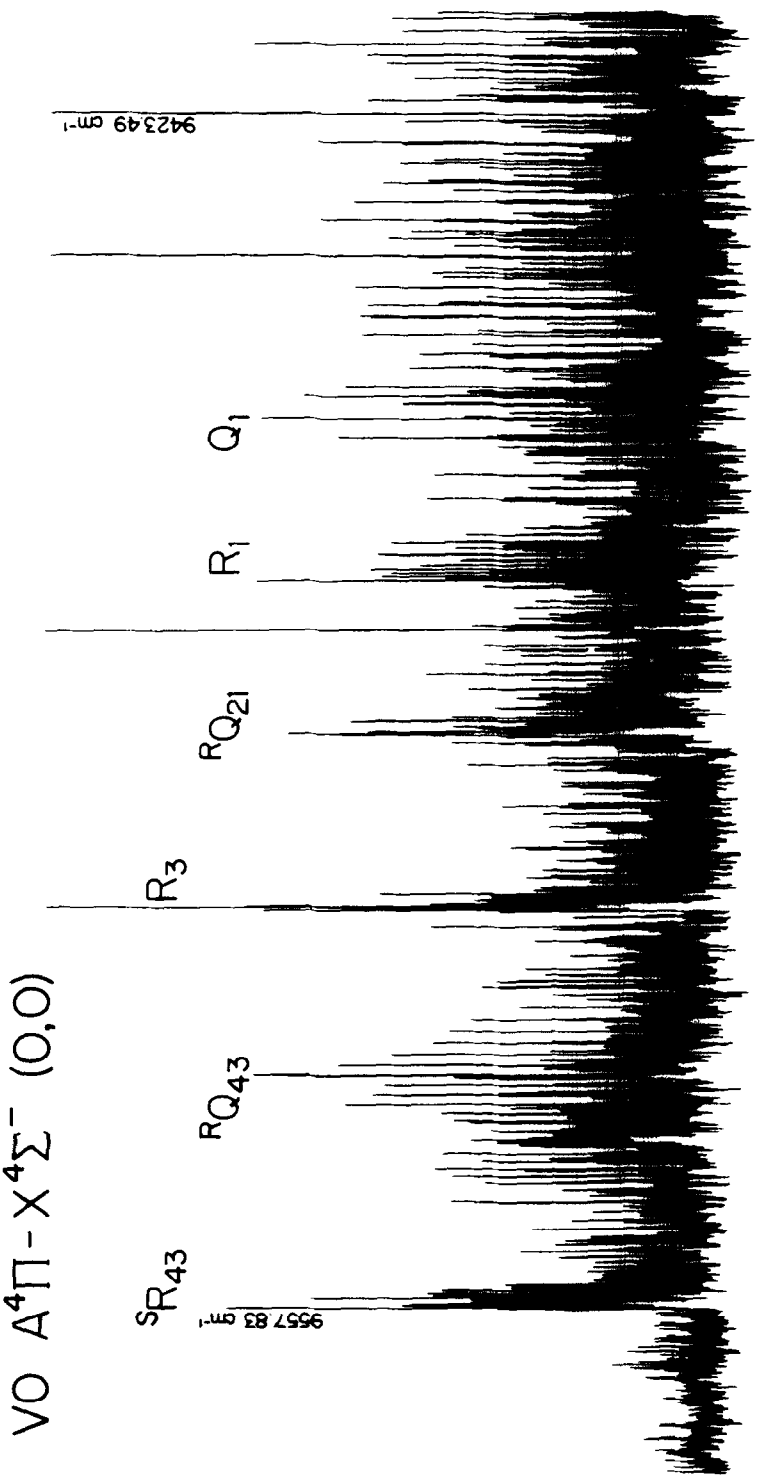

FIG. 1. Fourier transform spectrum of VO in the region 9410–9570 cm^{-1} showing the heads of the $A^4\Pi$–$X^4\Sigma^-$ (0, 0) band of VO.

second-order spin–orbit interactions, and the spin–rotation interaction, respectively, as

$$H = B(r)(\mathbf{J} - \mathbf{L} - \mathbf{S})^2 + A(r)\mathbf{L}\cdot\mathbf{S} + (2/3)\lambda(r)(3S_z^2 - \mathbf{S}^2) + \gamma(r)(\mathbf{J} - \mathbf{S})\cdot\mathbf{S}. \quad (1)$$

The expansion of the parameters A, B, λ, and γ, which are functions of the internuclear distance r, in terms of the normal coordinate, produces centrifugal distortion terms which are conveniently written in operator form as

$$H_{\text{c.d.}} = -D(\mathbf{J} - \mathbf{L} - \mathbf{S})^4 + (1/2)A_D[(\mathbf{J} - \mathbf{L} - \mathbf{S})^2, L_zS_z]_+ + (1/3)\lambda_D \times [(3S_z^2 - \mathbf{S}^2), (\mathbf{J} - \mathbf{L} - \mathbf{S})^2]_+ + (1/2)\gamma_D[(\mathbf{J} - \mathbf{L} - \mathbf{S})^2, (\mathbf{J} - \mathbf{S})\cdot\mathbf{S}]_+, \quad (2)$$

where $[x, y]_+$ means the anticommutator $xy + yx$, which is necessary to preserve Hermitian form for the matrices. The Λ doubling of the $^4\Pi$ state was calculated by setting up the 12×12 matrix for a $^4\Pi$ state interacting with a single $^4\Sigma^-$ state according to the first two terms of Eq. (1), applying a Wang transformation to convert to a parity basis and treating the elements off-diagonal in Λ by second-order perturbation theory. The effect is as if there were an operator

$$H_{\text{LD}} = (1/2)(o + p + q)(S_+^2 + S_-^2) - (1/2)(p + 2q) \times (J_+S_+ + J_-S_-) + (1/2)q(J_+^2 + J_-^2) \quad (3)$$

acting only within the manifold of the $^4\Pi$ state (*11*, *19*). The Λ-doubling parameters $(o + p + q)$, $(p + 2q)$, and q are related to matrix elements of the spin–orbit operator, as given in Ref. (*11*). The centrifugal distortion corrections to Eq. (3) are obtained in the same way that Eq. (2) is constructed from Eq. (1). The spin–spin operators $(1/2)\alpha(r)(S_+^2 + S_-^2)$ and $(2/3)\lambda^{(1)}(r)(3S_z^2 - S^2)$ are incorporated into the terms in $(o + p + q)$ and λ, respectively.

The resulting Hamiltonian matrices which we have used are given in Tables I and II (for $^4\Pi$ and $^4\Sigma$ states, respectively). The $X^4\Sigma^-$, $v = 0$ parameters were not varied in this work since they have been determined with great precision from the $C^4\Sigma^- - X^4\Sigma^-$ transition using sub-Doppler techniques (*17*). The parameter γ_S in the $^4\Sigma$ matrix represents the third-order spin–orbit contribution to the spin–rotation interaction (*16*, *17*); neither γ_S nor the centrifugal distortion correction γ_D appears in the $^4\Pi$ matrix because they are not needed.

Hyperfine effects have not been considered in Tables I and II because the hyperfine structure is not resolved. However, with the large spin and nuclear magnetic moment of ^{51}V ($I = 7/2$), the hyperfine structure is important in determining the details of the branch structure, as will be shown below.

5. ANALYSIS OF THE BRANCH STRUCTURE

Rather surprisingly, the analysis of the $A^4\Pi - X^4\Sigma^-$ bands of VO proved to be remarkably difficult because of unresolved hyperfine structure effects and overlapping sequence bands from the B–X transition. The problem with the hyperfine structure is that only when the hyperfine "widths" of the combining levels making up a rotational line are the same does the spectrum consist of sharp rotational lines (where the eight hyperfine transitions lie on top of each other). Since the four

TABLE I

Matrix Elements of the Rotational Hamiltonian for a $^4\Pi$ State in Case (a) Coupling

	$\lvert -\frac{1}{2}\rangle$	$\lvert \frac{1}{2}\rangle$	$\lvert \frac{3}{2}\rangle$	$\lvert \frac{5}{2}\rangle$
$\langle -\frac{1}{2}\rvert$	$T_{-\frac{1}{2}} + (B-\frac{3}{2}A_D+2\lambda_D)(z+1)$ $-D(z^2+5z+1)$ $\pm 3(J+\frac{1}{2})D_{o+p+q}$	$-\sqrt{3z}[B-\frac{1}{2}\gamma-A_D-2D(z+2)]$ $\mp\sqrt{3}[(o+p+q) + (z+2)D_{o+p+q}$ $+\frac{1}{2}(2z-1)D_{p+2q}]$	$-\sqrt{3(z-1)}\ [2D(J+\frac{1}{2})$ $\mp\frac{1}{2}(p+2q)\mp D_{o+p+q}$ $\mp\frac{1}{2}(z+1)D_{p+2q} \mp \frac{1}{2}(z-2)D_q]$	$\mp\sqrt{(z-1)(z-4)}\ [\frac{1}{2}q$ $+\frac{3}{2}D_{p+2q} + \frac{1}{2}D_q(z-2)]$
$\langle \frac{1}{2}\rvert$		$T_{\frac{1}{2}} + (B-\frac{1}{2}A_D-2\lambda_D)(z+3)$ $-D(z^2+13z+5)\pm(J+\frac{1}{2})[(p+2q)$ $+3D_{o+p+q} + D_{p+2q}(z+3)+D_q(z-1)]$	$-2\sqrt{z-1}[B-\frac{1}{2}\gamma-2\lambda_D-2D(z+2)$ $\pm\frac{1}{4}(J+\frac{1}{2})\{q+\frac{3}{2}D_{p+2q}$ $+D_q(z+2)\}]$	$\sqrt{3(z-1)(z-4)}\ [-2D$ $\pm\frac{1}{2}D_q(J+\frac{1}{2})]$
$\langle \frac{3}{2}\rvert$		Symmetric	$T_{3/2}+(B+\frac{1}{2}A_D-2\lambda_D)(z+1)$ $-D(z^2+9z-15)$ $\pm(z-1)(J+\frac{1}{2})D_q$	$-\sqrt{3(z-4)}\ [B-\frac{1}{2}\gamma+A_D$ $-2D(z-2)]$
$\langle \frac{5}{2}\rvert$				$T_{5/2}+(B+\frac{3}{2}A_D+2\lambda_D)(z-5)$ $-D(z^2-7z+13)$

$z = (J+\frac{1}{2})^2$. Upper and lower signs refer to e and f rotational levels respectively.

The basis functions $\lvert J\Omega\rangle$ have been abbreviated to $\lvert\Omega\rangle$

electron spin components of the ground state have hyperfine widths that differ from one to the next by about 0.2 cm^{-1}, rotational lines with the same upper state which go to different electron spin components of the ground state have noticeably different linewidths. The broader the linewidths the more the intensity is spread out,

TABLE II

Matrix Elements for Spin and Rotation in a $^4\Sigma^-$ State in Case (a) Coupling

	$\lvert \frac{3}{2}\rangle$	$\lvert \frac{1}{2}\rangle$
$\langle \frac{3}{2}\rvert$	$2\lambda + Bx - D(x^2+3x)$ $-\frac{3}{2}\gamma - 3\gamma_D x$	$-\sqrt{3x}[B-\frac{1}{2}\gamma-\gamma_S-\frac{1}{2}\gamma_D(x+7\mp\{2J+1\})$ $-2D(x+2)\mp\{J+\frac{1}{2}\})]$
$\langle \frac{1}{2}\rvert$	symmetric	$-2\lambda + B(x+4)-D[(x+4)^2+7x+4]$ $-\frac{7}{2}\gamma-\gamma_D(7x+16)$ $\mp 2[B-\frac{1}{2}\gamma-\frac{1}{2}\gamma_D(x+11)+\frac{3}{2}\gamma_S$ $- 2D(x+4)](J+\frac{1}{2})$

$x = (J+\frac{1}{2})^2-1$. Upper and lower signs give the e(F_1 and F_3) and f(F_2 and F_4) levels respectively. The basis functions $\lvert J\Sigma\rangle$ have been written $\lvert\Sigma\rangle$

and the more the line tends to get lost in the background of overlapping B–X structure. Therefore although a $^4\Pi$–$^4\Sigma^-$ transition should have 48 branches, most of them are broadened beyond recognition by the hyperfine structure in this case.

There are only two regions of clear branch structure in the (0, 0) band. One of these, shown in Fig. 2, lies between the two shortest wavelength heads. The obvious branch, later identified as $^RQ_{43}$, could be assigned at once to the F_3 spin component of the ground state because it contains the characteristic internal hyperfine perturbation pattern at $N'' = 15$ discovered by Richards and Barrow (*20*) in the B–X and C–X systems. This internal hyperfine perturbation is a remarkable occurrence, where the F_2 and F_3 electron spin components ($N = J - 1/2$ and $N = J + 1/2$, respectively) would cross at $N = 15$, because of the particular values of the rotational and spin parameters, were it not for the fact that they differ by one unit in J, and therefore interact through matrix elements of the hyperfine Hamiltonian of the type $\Delta N = \Delta F = 0$, $\Delta J = \pm 1$. Extra lines are induced, and, since the detailed course of the ground-state levels is known (*17*), their positions tell whether a branch containing them has F_2'' or F_3'', and also give its N numbering.

Given the numbering of the obvious F_3' branch, the other three F_4' branches marked in Fig. 2 could be numbered easily using ground state spin and rotational combination differences. The R_4 and Q_4 branches are hyperfine-broadened, and even though they are intrinsically strong they are by no means obvious in the spectrum. At this stage the lower states of the branches were known, but the nature of the upper state was still unclear.

The other region of obvious branch structure is the tail of the band, part of which is illustrated in Fig. 3. There are at least 10 sharp branches in this region, but only 8 of them actually belong to the A–X (0, 0) band. A further complication is that there are no ground-state combination differences connecting any of these 8. The analysis was performed by comparing the (0, 0) and (0, 1) bands, since the separations between corresponding (N, J) levels of the $X^4\Sigma^-$ $v = 0$ and 1 levels are known from the analysis of the C–X system (*21*). This method gives at most two possible N numberings for the branches, but it is less easy to determine the ground-state spin component since the intervals are very nearly the same for the four spin components. Eventually all 8 of these branches were identified, and assigned to their respective ground-state spin components. The resulting pattern can be interpreted as the Q and P main branches of a $^4\Pi$–$^4\Sigma$ transition where the $^4\Pi$ state is close to case (*b*) coupling at these high-N values, and all four components show Λ doubling. The analysis is confirmed by the identification of the four R branches, and various weak hyperfine-broadened spin satellite branches.

The Q_4 branch is interesting because it is a sharp branch at the high N values of Fig. 3, but hyperfine-broadened at the lower N values of Fig. 2. It is possible to follow the Q_4 branch over the complete range of N values, and to see how it changes from broad to narrow fairly quickly in the region $N = 40$–50. The reason for the sudden disappearance of the $^RQ_{43}$ branch near $N = 35$ (see Fig. 2) is then clear—the $^RQ_{43}$ branch is prominent at low N because the hyperfine structure of the $^4\Pi$ F_4 level is initially the same as that of the $X^4\Sigma^-$ F_3 level, but with increasing N spin-uncoupling changes the $^4\Pi$ hyperfine level pattern until at high N it becomes the same as $X^4\Sigma^-$ F_4; as a result the $^RQ_{43}$ branch becomes broadened. In addition

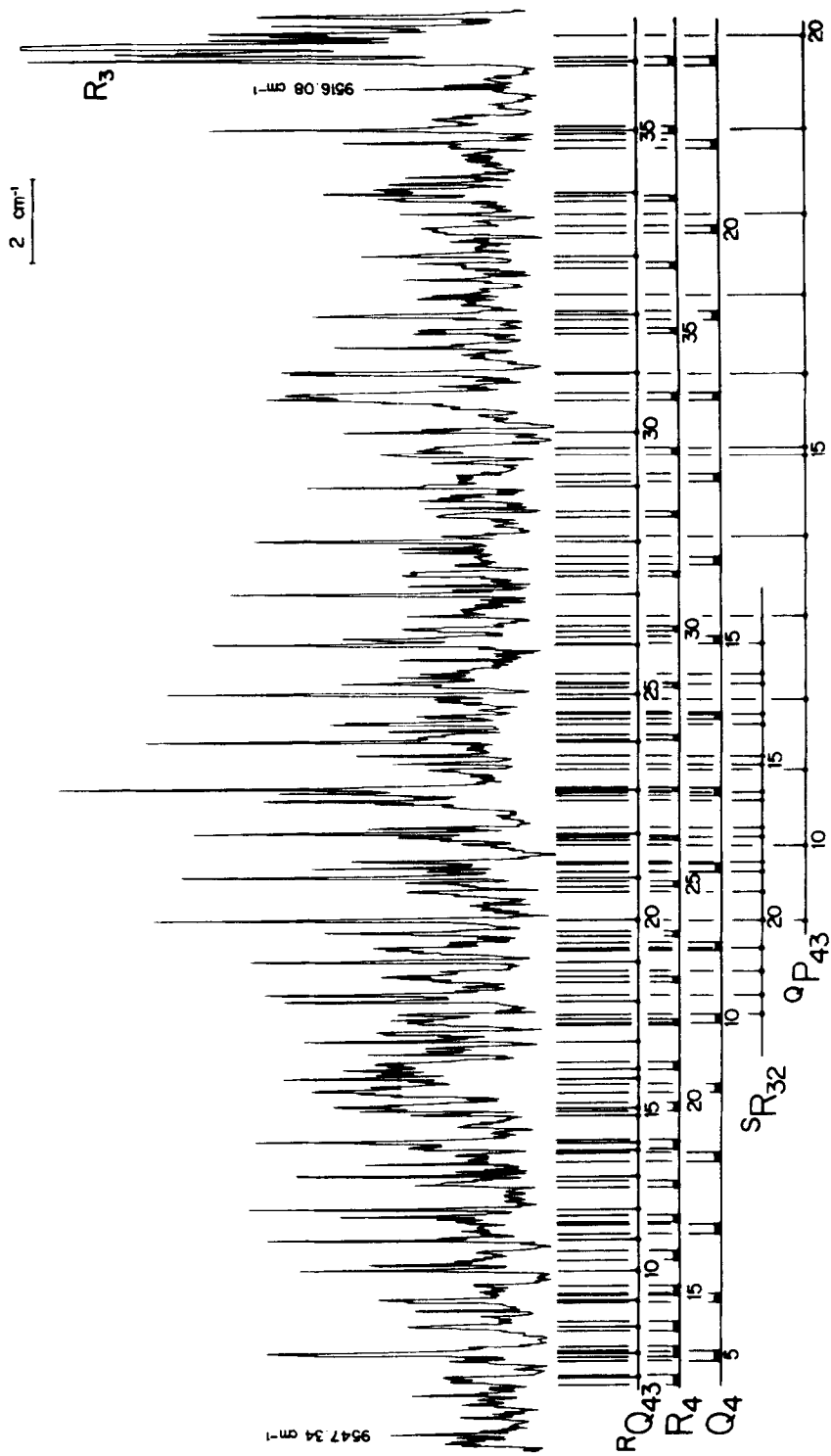

FIG. 2. Rotational structure in the $A^4\Pi$–$X^4\Sigma^-$ (0, 0) band of VO, showing the F'_4 branch structure ($^4\Pi_{5/2}$).

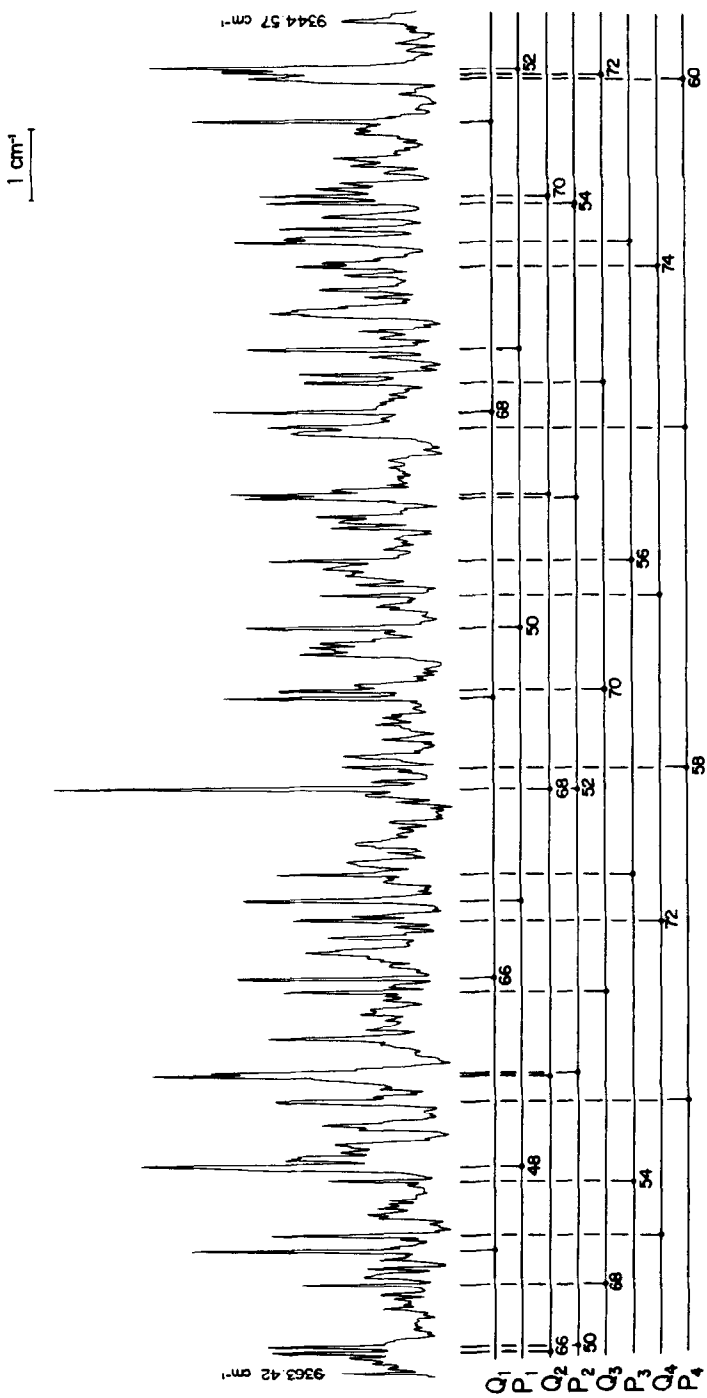

FIG. 3. High-N main branch Q and P lines in the tail of the VO $A^4\Pi$–$X^4\Sigma^-$ (0, 0) band.

the intensity of ${}^{R}Q_{43}$, which is a spin satellite branch that becomes forbidden in a ${}^4\Pi(b)$–${}^4\Sigma(b)$ transition, must diminish as spin-uncoupling sets in.

What emerges finally is a "textbook" example of a ${}^4\Pi_r$–${}^4\Sigma$ transition where the ${}^4\Pi$ state has quite small spin–orbit coupling so that it changes fairly quickly from case (a) to case (b) coupling. The ${}^4\Pi$ state is shown to be regular (with a positive spin–orbit coupling constant) because there is no detectable Λ doubling in the F_4 component (${}^4\Pi_{5/2}$) before about $N = 45$, whereas the other three spin components show Λ-doubling effects almost from their first levels. The Λ-doubling and spin-uncoupling patterns are shown qualitatively in Fig. 4, where the upper-state energy levels, suitably scaled, are plotted against $J(J + 1)$. The curvature in the plots of Fig. 4 is a consequence of the spin-uncoupling. The assigned lines of the (0, 0) and (0, 1) bands of the A–X system are given in the Appendix; only the sharp lines are listed, because they are sufficient to determine the upper-state constants, and in any case it is often quite difficult to obtain the exact line centres for the hyperfine-broadened branches.

6. LEAST-SQUARES FITTING OF THE DATA

One of the unexpected effects of the ground-state internal hyperfine perturbation is that the F_2'' and F_3'' levels are appreciably shifted from the positions that they would have in the absence of hyperfine structure. Therefore it is necessary to correct all the line positions in the branches involving F_2 or F_3 lower levels for this effect.

It may seem surprising that a hyperfine effect can shift the positions of rotational levels, but the hyperfine matrix element acting between F_2 and F_3 levels with the same N value is about 0.08 cm^{-1}, while the zero-order separation of the F_2 and F_3

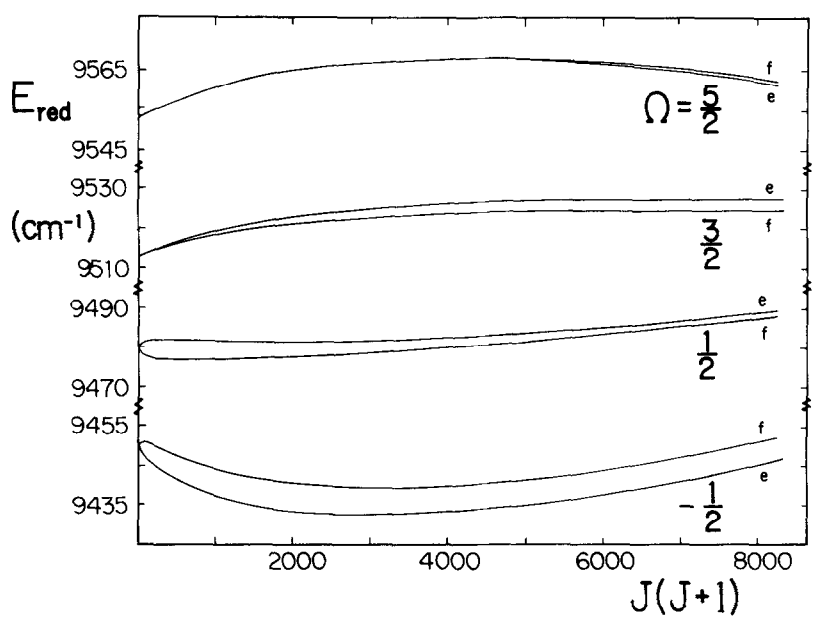

FIG. 4. Reduced energy levels of the $A^4\Pi$ state of VO plotted against $J(J + 1)$. The quantity plotted is the upper-state term value less $(0.50865 + 0.00365\Omega)(J + 1/2)^2 - 6.7 \times 10^{-7}(J + 1/2)^4$ cm^{-1}.

TABLE III

Corrections Applied to the Observed F_2 and F_3 Line Positions to Allow for the Internal Hyperfine Perturbation Shifts

N	F_2	F_3	N	F_2	F_3	N	F_2	F_3
4	-0.030	-0.003	14	-0.079	+0.055	24	+0.029	-0.026
5	-0.031	+0.008	15	±0.080		25	0.027	-0.025
6	-0.031	0.012	16	+0.075	-0.086	26	0.026	-0.024
7	-0.033	0.017	17	0.065	-0.075	27	0.025	-0.022
8	-0.034	0.022	18	0.051	-0.060	28	0.023	-0.021
9	-0.036	0.025	19	0.047	-0.058	29	0.023	-0.020
10	-0.053	0.031	20	0.043	-0.043	30	0.022	-0.019
11	-0.060	0.033	21	0.038	-0.039	31	0.021	-0.018
12	-0.065	0.034	22	0.035	-0.031	32	0.021	-0.018
13	-0.070	0.043	23	0.032	-0.028	33	0.020	-0.017

The corrections were obtained by subtracting the rotational energy calculated in the absence of hyperfine effects from a weighted average of the rotational-hyperfine energies given by a full calculation of the hyperfine structure.

levels (which depends on the spin–rotation parameter γ) remains less than 1 cm^{-1} even some distance from the N value of the internal perturbation. The calculated shifts are given in Table III.

After applying these corrections to the F_2'' and F_3'' branches we fitted the lines directly to the appropriate differences between eigenvalues of the $^4\Pi$ and $^4\Sigma^-$ matrices. No attempt was made to vary the $X^4\Sigma^-$, $v = 0$ parameters in the present work since they have been determined with high precision by the sub-Doppler spectra of (*17*), where the resolution is a factor of 10 higher. Our procedure is therefore equivalent to fitting the term values of the $A^4\Pi$, $v = 0$ state to the eigenvalues of Table I. The (0, 1) band was then fitted similarly, but with the $A^4\Pi$ upper-state parameters fixed at the values derived from the (0, 0) band; the results give essentially the differences between the parameters for $X^4\Sigma^-$ $v = 0$ and $v = 1$.

The final parameters are assembled in Table IV. The overall standard deviations listed correspond to unit weighting of all the data; they are not as low as we had expected, but in view of the blending and the unusual lineshapes produced by unresolved hyperfine structure effects in some of the branches we see no reason for concern.

7. DISCUSSION

(i) Spin–Orbit Coupling Constants and Indeterminacies

Since $^4\Pi$ states are comparatively uncommon it is instructive to see what parameters can be determined in this case, and what happens to the problem of the indeterminacy of some of the parameters in the general case.

TABLE IV

Parameters Derived from Rotational Analysis of the $A^4\Pi$–$X^4\Sigma^-$ (0, 0) and (0, 1) Bands of VO (cm^{-1})

$A^4\Pi$, v = 0			$X^4\Sigma^-$, v = 0		v = 1	
$T_{5/2}$	9555.500	±0.011 (3σ)	T_0	0	1001.812	±0.011 (3σ)
$T_{3/2}$	9512.432	±0.017	B	0.546383_3	0.542864	±0.000013
$T_{1/2}$	9477.830	±0.023	10^7D	6.509	6.54	±0.03
$T_{-1/2}$	9449.710	±0.021	λ	2.0308_7	2.028	±0.002
B	0.516932	±0.000006	γ	0.02251_6	0.0226	fixed
10^7D	6.782	±0.010	$10^5\gamma_S$	-1	-1	fixed
q	-0.000151	±0.000012	$10^8\gamma_D$	5.6	5.6	fixed
p+2q	-0.01349	±0.00027		fixed		
o+p+q	2.107	±0.008				
γ	0.00383	±0.00010				
10^7D_q	0.023	±0.022				
10^7D_{p+2q}	-2.32	±0.68				
10^5D_{o+p+q}	-4.95	±0.42				
λ_D	0.000050	±0.000004				

Standard deviations (unit weight):- $A^4\Pi$, v = 0: 0.024 cm^{-1}; $X^4\Sigma^-$, v = 1: 0.024 cm^{-1}

Bond lengths: $A^4\Pi$, r_0 = 1.6368 Å; $X^4\Sigma^-$, r_0 = 1.5920 Å, r_e = 1.5894 Å

($B_e = 0.54814_3$, $\alpha_e = 0.00351_9$ cm^{-1})

Veseth (*21*) has pointed out how γ and A_D (the spin–rotation interaction and the centrifugal distortion correction to the spin–orbit coupling) cannot be determined separately in a $^2\Pi$ state, and Brown *et al.* (*19*) have proved this rigorously. Brown *et al.* have also shown that an indeterminacy exists among B, A_D, λ_D, and γ for case (*a*) $^3\Pi$ states, essentially because there are only three effective B values for the three spin–orbit components, but four parameters to be determined from them. The indeterminacy can be avoided if the levels can be followed to high J values, where case (*b*) coupling applies, because there is additional information in the effective D values of the three spin–orbit components. No such indeterminacy occurs for $^4\Pi$ states because there are now four effective B values to determine the same four parameters; only if higher-order terms such as γ_S (the third-order spin–orbit correction to the spin-rotation interaction (*16*, *17*)) are needed will further indeterminacies arise.

It is very clear from our data that A_D is effectively zero for the $A^4\Pi$ state of VO. If A_D is floated the standard deviation *increases* marginally, and A_D is given as $(4 \pm 12) \times 10^{-6}$ cm^{-1}. Nevertheless if it were not so small it would in principle have been determinable from the data.

Another indeterminacy may arise in the substate origins for the components of a multiplet Π state. These origins can be expressed, in terms of the spin–orbit and spin–rotation parameters, as

$$T_\Omega = T_0 + A\Lambda\Sigma + (2/3)\lambda[3\Sigma^2 - S(S+1)] + \gamma[\Omega\Sigma - S(S+1)] + \eta\Lambda[\Sigma^3 - (3S^2 + 3S - 1)\Sigma/5], \quad (4)$$

where η is the third-order spin–orbit interaction (*22*, 23). From the previous discussion it is seen that for a $^3\Pi(a)$ state only effective values of T_0, A, and λ can be determined, but that all five parameters can be determined for a $^4\Pi$ state, because γ can be obtained from the rotational structure.

Because γ has to be determined separately we have written the substate origins in Tables I and IV in the form of T_Ω values. However, it would be entirely equivalent to use expressions derived from Eq. (4) in the least-squares work. Converting from the T_Ω values given in Table IV we have

$$\begin{aligned} T_0 &= 9498.878\ \text{cm}^{-1}; & A &= 35.193\ \text{cm}^{-1}, \\ \lambda &= 1.867\ \text{cm}^{-1}; & \eta &= 0.331\ \text{cm}^{-1}. \end{aligned} \quad (5)$$

It is interesting to see how comparatively large the second-order parameter λ is compared to A. As is well known (*18*) the second-order parameter λ includes the diagonal spin–spin interaction, but since the latter cannot be estimated easily it is not possible to say how much of the observed λ is caused by it. The observed λ for the $A^4\Pi$ state is similar to that for the $X^4\Sigma^-$ state (see Table IV), so that its large size is not unexpected. To our knowledge an accurate value of the third-order parameter η has only previously been obtained for the level $v = 4$ of the $^4\Pi_u$ state of O_2^+ (*23*), though estimates have been made for the $A^5\Pi$ and $X^5\Pi$ states of CrO (*22*).

(ii) Λ-Doubling Parameters

In the approximation where a single $^4\Sigma^-$ state causes the Λ-doubling in a $^4\Pi$ state the parameters o, p, and q are given by

$$\begin{aligned} o &= -(1/2)\langle {}^4\Pi|AL_+|{}^4\Sigma^-\rangle^2/\Delta E_{\Pi\Sigma}, \\ p &= -2\langle {}^4\Pi|AL_+|{}^4\Sigma^-\rangle\langle {}^4\Pi|BL_+|{}^4\Sigma^-\rangle/\Delta E_{\Pi\Sigma}, \\ q &= -2\langle {}^4\Pi|BL_+|{}^4\Sigma^-\rangle^2/\Delta E_{\Pi\Sigma}. \end{aligned} \quad (6)$$

Two approximate relations between the Λ-doubling parameters follow at once:

$$p/q = A/B \quad (7)$$

and

$$p^2 = 4oq. \quad (8)$$

Equation (7) should in fact be obeyed quite well no matter what the states causing the Λ doubling are because it assumes only that the matrix elements of AL_+ and BL_+ are in the ratio of A to B; from Table IV we find

$$(p/q)/(A/B) = 1.26 \tag{9}$$

which is not far from unity. Equation (8) on the other hand is not obeyed at all, and the experimental ratio $p^2/4oq$ is −0.13. There are two possible reasons. One is that the off-diagonal spin–spin interaction parameter α (which should be subtracted from the expression for o in Eq. (6)) is important; the other, which is rather more likely, is that there is a nearby strongly interacting electronic state of different multiplicity. Assuming that the spin–orbit operator is responsible, such a state will have rotation-independent matrix elements with $A^4\Pi$, so that it will contribute to the parameter o, but not to p or q.

As far as we can tell from our spectra the $A^4\Pi$, $v = 0$ level is unperturbed rotationally, and the principal perturbations in $B^4\Pi$ are by another $^4\Sigma^-$ state; however, there is evidence (*17*) for a $^2\Pi$ state perturbing $C^4\Sigma^-$, $v = 0$ (at 17 420 cm^{-1}), which possibly comes from the same electron configuration as $A^4\Pi$ and is a good candidate for causing the effects described.

(iii) Hyperfine Structure of the $A^4\Pi$ State

Section 5 described how the main branches ($\Delta N = \Delta J$) in all four $^4\Pi$–$^4\Sigma^-$ subbands become "sharp" at high N values (where the spin coupling approximates

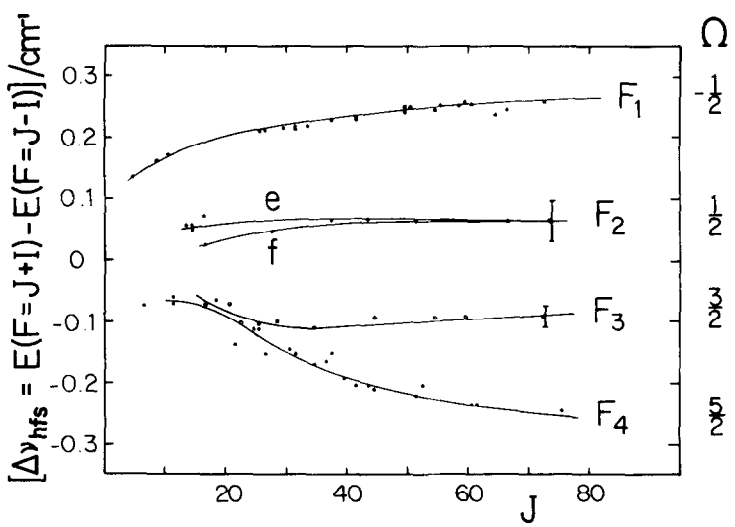

FIG. 5. Hyperfine widths, $\Delta E_{hfs} = E_{hfs}(F = J + I) - E_{hfs}(F = J - I)$, of the four spin components of the $A^4\Pi$ state of VO, plotted against J. Points are widths calculated from the ground-state hyperfine structure and the observed linewidths, without correction for the Doppler width.

case ($b_{\beta J}$) in both states) although they are often hyperfine-broadened at low N. It has been possible to obtain the approximate hyperfine widths of the four components of $A^4\Pi$ from detailed measurements of the lineshapes in the various branches, together with the known hyperfine structure of the ground state (*17*); the results are shown in Fig. 5. This figure should be considered only as an "artist's impression" because the hyperfine structure is never resolved in the $A^4\Pi$–$X^4\Sigma^-$ transition, and the deconvolution of the Doppler and hyperfine profiles has not been attempted. The error bars given for the F_2 and F_3 components show that it is relatively futile to try to obtain values for any of the hyperfine parameters except b, but on the other hand the value of b can be obtained with reasonable accuracy.

To understand why only the hyperfine parameter b is determinable we consider the magnetic hyperfine Hamiltonian (*24*) in detail:

$$H_{\text{mag.hfs}} = a\mathbf{I}\cdot\mathbf{L} + b\mathbf{I}\cdot\mathbf{S} + cI_zS_z + (1/2)d(e^{2i\phi}I_-S_- + e^{-2i\phi}I_+S_+). \quad (10)$$

In this equation the first term is the interaction between the electron orbital motion and the nuclear spin, the second term is a combination of the Fermi contact interaction and the dipolar interaction, and the last two terms are dipolar interactions, respectively diagonal and off-diagonal in Λ in a signed quantum number basis. The term in d gives rise to different hyperfine structures in the two Λ-doubling components of $^4\Pi_{1/2}$, and its effects can be seen in Fig. 5, where there is a definite difference between the hyperfine widths of the F_{2e} and F_{2f} levels up to about $J = 50$. This difference can be measured fairly accurately because the linewidths in the P_2 and Q_2 branches are quite obviously different, though the absolute values of the hyperfine widths are uncertain to the extent of the error bars in Fig. 5.

In case (a_β) coupling the diagonal matrix elements (*25*) of the first three terms of Eq. (10) are

$$\langle J\Omega\Lambda IF|H_{\text{hfs}}|J\Omega\Lambda IF\rangle = [F(F+1) - I(I+1) - J(J+1)]\Omega[a\Lambda + (b+c)\Sigma]/[2J(J+1)], \quad (11)$$

while the d term contributes $\pm d(S+1/2)(J+1/2)[F(F+1) - I(I+1) - J(J+1)]/[4J(J+1)]$ to the diagonal elements for $\Omega = 1/2$ when S is half-integral. The hyperfine widths (in other words the separations of the hyperfine components with $F = J + I$ and $F = J - I$) for a $^4\Pi$ state, where $I = 7/2$, are therefore

$$\Delta E_{\text{hfs}} = 7(J+1/2)\Omega[a + (b+c)\Sigma]/[J(J+1)] \pm 7(J+1/2)^2 d\delta_{\Omega,1/2}/[J(J+1)]. \quad (12)$$

Equation (12) implies that the hyperfine widths should decrease as $1/J$ except that there is a J-independent contribution of $\pm 7d$ in the two Λ components of $^4\Pi_{1/2}$.

In case ($b_{\beta J}$), on the other hand, the diagonal matrix elements of the magnetic hyperfine Hamiltonian are

$$\langle N\Lambda SJIF|H_{\rm hfs}|N\Lambda SJIF\rangle$$
$$= \frac{[F(F+1) - I(I+1) - J(J+1)]}{4J(J+1)} \left\{ \frac{a\Lambda^2 X(NJS)}{N(N+1)} + bX(JSN) \right.$$
$$- \frac{c[3\Lambda^2 - N(N+1)][3X(SNJ)X(NJS) + 2X(JSN)N(N+1)]}{3N(N+1)(2N-1)(2N+3)}$$
$$\left. \pm \frac{d[3X(SNJ)X(NJS) + 2X(JSN)N(N+1)]}{2(2N-1)(2N+3)} \delta_{|\Lambda|,1} \right\}, \qquad (13)$$

where $X(xyz) = x(x+1) + y(y+1) - z(z+1)$. It is not so easy to see the J dependence in these formulas, but order-of-magnitude considerations show that the coefficients of a and c decrease as $1/J$, while the coefficients of b and d are almost independent of J. The hyperfine energy expressions for $^4\Pi(b)$ states are roughly

$$F_1(J = N + 3/2)\ E_{\rm hfs} = -(3/2)(b \pm (1/4)d)X(JIF)/(2N+3),$$

$$F_2(J = N + 1/2) \qquad -(1/2)(b \pm (1/4)d)X(JIF)(2N+9)/[(2N+1)(2N+3),$$

$$F_3(J = N - 1/2) \qquad (1/2)(b \pm (1/4)d)X(JIF)(2N-7)/[(2N-1)(2N+1)],$$

$$F_4(J = N - 3/2) \qquad (3/2)(b \pm (1/4)d)X(JIF)/(2N-1), \qquad (14)$$

where the terms in $\pm(1/4)d$ refer to the Λ-doubling components; for $I = 7/2$ the approximate hyperfine widths in the four spin components, in units of $7(b \pm (d/4)/2$, are 3, 1, -1, and -3, respectively.

Figure 5 shows that the hyperfine patterns in the $A^4\Pi$ state of VO, over the range $J = 10$–80, correspond to a spin coupling intermediate between cases (a_β) and ($b_{\beta J}$). As described above, the different hyperfine widths in the F_{2e} and F_{2f} components represent the dipolar d term, but the observed difference is a complicated function of how far the spin-uncoupling has proceeded. The d term should show up again as a small difference between the Q and P branch widths for the high-N F_1 and F_4 lines, but this is not observable at our resolution. The high-N pattern corresponds to almost pure case ($b_{\beta J}$) coupling, with the parameter b being very nearly the same as that in the ground state (hence the "sharp" main branch lines where the hyperfine components all fall on top of one another). The experimental value of b is

$$b(A^4\Pi) = +0.026 \pm 0.002\ {\rm cm}^{-1} \qquad (15)$$

compared to the ground-state value 0.02731 ± 0.00004 cm^{-1} (*17*).

We have not attempted to obtain values for a, c, and d, from Fig. 5, since the pattern is clearly dominated by the parameter b, with the exact details being governed by the extent of the spin-uncoupling.

The fact that $b(A^4\Pi)$ is closely similar to $b(X^4\Sigma^-)$ indicates that the same $4s\sigma$ electron responsible for the Fermi contact interaction in the ground state is also present in the $A^4\Pi$ state. In single configuration approximation the electron configurations must therefore be

$$X^4\Sigma^- : (4s\sigma)^1(3d\delta)^2, \qquad A^4\Pi : (4s\sigma)^1(3d\delta)^1(4p\pi)^1. \tag{16}$$

The configuration given for $A^4\Pi$ also produces a $^4\Phi$ state, which should lie at still lower energy; the chances of observing it appear slim at present since its Λ value differs by at least two units from all the other known states of VO.

APPENDIX

Rotational Lines Assigned to the $A^4\Pi$–$X^4\Sigma^-$ Transition of VO (cm^{-1})

APPENDIX (i)

(0, 0) Band

N	P1	Q1	R1	P2	Q2	R2	P3	Q3
8		9463.781*						
9		9464.329						
10		9464.857						
11								
12		9465.522*						
13			9475.676*					
14	9445.053		9476.479*					9499.634*
15	9443.808		9477.192*	9459.359				9498.535)
								98.348)
16	9442.432*	9465.573*	9477.857*	9457.662	9479.218			9497.349)
								97.147)
17	9441.077	9465.484*	9478.474*	9455.897	9478.572*			9496.124
18	9439.591	9464.989*	9478.989*	9454.010	9477.857*			9494.847
19	9438.053	9464.642	9479.453*	9452.210*	9477.042			9493.540
20	9436.339*	9464.051	9479.817*	9450.217*	9476.164			9492.169
21	9434.673	9463.383*	9480.116*	9448.210*	9475.195			9490.751
22	9432.846*	9462.702*	9480.343*	9446.150*	9474.189			9489.272*
23	9430.936*	9461.873*	9480.501	9444.080	9473.095			9487.782*
24	9428.994*	9460.968*	9480.626*	9441.903	9471.922	9493.023	9462.440	9486.195*
25	9426.963	9460.014*	9480.626*	9439.537*	9470.674	9492.829	9459.841	9484.581
26	9424.883*	9459.029*	9480.572*	9437.343	9469.360	9492.616	9457.208	9482.915
27	9422.725*	9457.860*	9480.343*	9434.997*	9467.977	9492.253	9454.513	9481.180
28	9420.476*	9456.680*	9480.116*	9432.560	9466.521	9491.868*	9451.765	9479.411
29	9418.133	9455.394*	9479.817*	9430.044	9464.989	9491.424	9448.978*	9477.573
30	9415.714	9454.010	9479.453*	9427.502	9463.383*	9490.920*	9446.052*	9475.676
31	9413.245	9452.588	9478.989*	9424.883*	9461.723	9490.334*	9443.213	9473.750
32	9410.705*	9451.041	9478.474*	9422.199	9460.014*	9489.693	9440.251	9471.748*
33	9408.076	9449.435	9477.857*	9419.535*	9458.218	9488.950*	9437.235	9469.707
34	9405.384	9447.786	9477.192*	9416.649	9456.360	9488.220	9434.157	9467.606
35	9402.600*	9446.052*	9476.479*	9413.773	9454.426	9487.380*	9431.023	9465.448*
36	9399.787	9444.214	9475.676*	9410.834	9452.434*	9486.472*	9427.851	9463.238*
37	9396.867	9442.319	9474.779	9407.808	9450.382	9485.578	9424.644*	9460.968*
38	9393.899	9440.361	9473.838	9404.777	9448.237	9484.483*	9421.311	9458.634
39	9390.879*	9438.324	9472.819	9401.649	9446.052*	9483.415*	9417.932	9456.247
40	9387.752	9436.218	9471.748	9398.462	9443.808	9482.232	9414.516*	9453.812
41	9384.577	9434.042	9470.590	9395.189	9441.491	9481.006	9411.067*	9451.317*
42	9381.333	9431.796	9469.360*	9391.881	9439.113	9479.723	9407.538	9448.764
43	9378.035*	9429.482	9468.058	9388.488	9436.667	9478.358	9403.951*	9446.150*
44	9374.641	9427.096	9466.708	9385.048	9434.157	9476.932*	9400.301	9443.492
45	9371.193	9424.644	9465.275	9381.535*	9431.588	9475.503	9396.600	9440.773
46	9367.675	9422.120	9463.781	9377.964*	9428.948	9473.898*	9392.844	9437.992
47	9364.110	9419.535	9462.220	9374.325	9426.253	9472.292*	9389.018	9435.145
48	9360.455*	9416.869*	9460.587*	9370.603	9423.490*	9470.590*	9385.143	9432.255
49	9356.743	9414.154	9458.895	9366.856	9420.660	9468.870*	9381.213	9429.303
50	9352.965	9411.366	9457.132	9363.009	9417.755	9467.046	9377.203	9426.295

APPENDIX (i)

N	P1	Q1	R1	P2	Q2	R2	P3	Q3
51	9349.124	9408.512	9455.313	9359.144	9414.818	9465.175	9373.172	9423.236
52	9345.218	9405.596	9453.403	9355.179	9411.812	9463.238*	9369.059	9420.106
53	9341.248	9402.600*	9451.458	9351.164	9408.719	9461.240	9364.889	9416.869*
54	9337.209	9399.548	9449.435*	9347.089	9405.596*	9459.180	9360.665	9413.659
55	9333.103	9396.427	9447.330*	9342.949	9402.396	9457.047	9356.385	9410.379
56	9328.940	9393.239	9445.170	9338.733*	9399.145	9454.856	9352.043	9407.024
57	9324.708	9389.992	9442.940	9334.482	9395.812	9452.588*	9347.637	9403.604
58	9320.412	9386.677	9440.648	9330.137*	9392.429	9450.273*	9343.180	9400.126
59	9316.061*	9383.295	9438.324*	9325.763*	9388.982	9447.863*	9338.663	9396.600*
60	9311.634	9379.847*	9435.887*	9321.306	9385.467*	9445.437	9334.087*	9393.001
61	9307.134	9376.340	9433.386	9316.793	9381.901	9442.940*	9329.456	9389.348
62	9302.600	9372.771	9430.837		9378.277	9440.361*	9324.756	9385.643
63	9297.979*	9369.130	9428.212		9374.573	9437.712	9320.012*	9381.901*
64	9293.298	9365.424	9425.497		9370.820	9434.987*	9315.194*	9378.035
65	9288.569	9361.658	9422.785		9366.984	9432.233*	9310.325*	9374.158
66	9283.764	9357.811*	9419.979		9363.124	9429.386	9305.433*	9370.209
67	9278.906	9353.937			9359.184	9426.454*	9300.415*	9366.201
68	9273.976	9349.976			9355.179	9423.490*	9295.368	9362.139
69	9268.980	9345.925			9351.123		9290.247	9358.013
70	9263.925	9341.849			9346.994			9353.827
71	9258.810	9337.715			9342.808			9349.565
72		9333.503			9338.563			9345.277
73		9329.220*			9334.248			9340.922
74		9324.885			9329.879			9336.500
75		9320.490			9325.454			9332.017
76		9316.024			9320.963			
77		9311.484			9316.410			
78		9306.889			9311.793			
79		9302.240						
80		9297.529						
81		9292.724						
82		9287.905						
83		9282.998						
84		9278.036						
85		9273.010						
86		9267.920						
87		9262.779						
88		9257.507						

APPENDIX (i)

N	R3	P4	Q4	R4	QP43	RQ43	SR43
4							9552.881
5							9553.306
6						9546.923*	9553.904
7						9546.320*	9554.335
8						9545.672*	9554.829*
9						9545.003*	9555.197*
10						9544.291*	9555.563*
11					9532.315	9543.567	9555.897
12					9530.485*	9542.805	9556.205
13					9528.632	9542.020	9556.476
14					9526.736	9541.188*	9556.712*
15					9525.020)	9540.533)	9556.930)
					24.806)*	40.311)*	57.183)
16	9515.097					9539.649	9557.314
17	9514.934				9521.083	9538.740	9557.465
18	9514.842				9519.094	9537.793	9557.583*
19	9514.596				9517.073*	9536.841	9557.705*
20	9514.365					9535.880	9557.795*
21	9514.067				9512.963*	9534.857	9557.823*
22	9513.716				9510.867	9533.818	9557.823*
23	9513.335				9508.741	9532.750	9557.823*
24	9512.830				9506.581	9531.644	9557.795*
25	9512.313				9504.387	9530.485*	9557.705*
26	9511.738				9502.169*	9529.314	9557.583*
27	9511.148*				9499.901	9528.121	9557.428
28	9510.446				9497.616*	9526.880	9557.231
29	9509.703					9525.597	9556.997
30	9508.911	9467.217*				9524.274	9556.712*
31	9508.062	9463.781*				9522.908	9556.404
32	9507.159	9460.348*				9521.514	9556.057
33	9506.199	9456.809*				9520.077	9555.563*
34	9505.178	9453.282*				9518.593	
35	9504.100	9449.685		9521.901*		9517.073*	
36	9502.964	9446.052		9520.250*		9515.501*	
37	9501.772	9442.436*	9480.116*	9518.718*		9513.899*	
38	9500.521	9438.691	9477.400*	9517.073*		9512.223*	
39	9499.205	9434.928*	9474.642	9515.406*		9510.534*	
40	9497.835	9431.146	9471.922	9513.716*			
41	9496.408	9427.349	9469.112	9511.923*			
42	9494.918	9423.490*	9466.306	9510.126*			
43	9493.376	9419.535*	9463.383*	9508.293*			
44	9491.777	9415.536	9460.445*	9506.331			
45	9490.103	9411.499	9457.464*	9504.387*			
46	9488.378	9407.446	9454.426*	9502.375*			
47	9486.591	9403.330	9451.317*	9500.323			
48	9484.752	9399.199	9448.172	9498.213			
49	9482.838	9395.007	9444.985	9496.028*			
50	9480.877	9390.728	9441.746	9493.844*			

APPENDIX (i)

N	R3	P4	Q4	R4	N	PQ13	SR32
51	9478.859	9386.394	9438.425	9491.584	4	9448.699	
52	9476.779	9382.035	9435.104	9489.272*	5	9448.303	
53	9474.642	9377.667*	9431.705	9486.908	6	9447.863*	
54	9472.422	9373.172	9428.260	9484.483*	7	9447.330*	
55	9470.167	9368.694	9424.770	9482.031	8	9446.731	
56	9467.836	9364.110*	9421.213	9479.453*	9		
57	9465.448*	9359.534	9417.620	9476.932*	10	9445.276	
58	9463.006	9354.888	9413.962	9474.295*	11	9444.427	
59	9460.511	9350.189	9410.254	9471.619	12	9443.497*	
60	9457.860*	9345.365*	9406.486	9468.870*	13		
61	9455.313*	9340.672*	9402.664	9466.090	14		9531.011
62	9452.588*	9335.757	9398.791	9463.238*	15		9531.965
63	9449.857	9330.827	9394.869	9460.345*	16		9532.856
64	9447.071*	9325.819	9390.879*	9457.417*	17		9533.688
65	9444.214*	9320.823	9386.844	9454.361*	18		9534.481
66	9441.311*	9315.761	9382.762	9451.291*	19		9535.213
67			9378.609	9448.164*	20		9535.880*
68			9374.407	9444.980*	21		9536.525
69			9370.143	9441.740*	22		9537.105
70			9365.826	9435.088*	23		9537.649*
71			9361.447	9431.676*	24		9538.104
72			9357.012	9428.207*			
73			9352.527				
74			9347.977	9421.117*			
75			9343.379	9417.452			
76			9338.733*	9413.773*			
77			9334.000				
78			9329.228*	9406.190			
79			9324.393	9402.337*			
80			9319.494	9398.380			
81			9314.542	9394.382			
82			9309.530	9390.327			
83			9304.461	9386.202			
84			9299.336	9382.035*			
85			9294.143	9377.794			
86			9288.901				
87			9283.597				
88			9278.224				
89			9272.797				
90			9267.312				
91			9261.786				

APPENDIX (ii)

(0, 1) Band

N	P1	Q1	R1	P2	Q2	Q3	R3	RQ43	SR43
7		8461.506							
8		8462.320						8544.072*	8553.232
9		8462.959						8543.503*	8553.720*
10		8463.595					8513.337*	8542.869	8554.122
11		8463.987					8513.525	8542.216	8554.542
12		8464.292*					8513.756	8541.537	8554.940*
13		8464.613*					8513.980*	8540.840	8555.340
14		8464.803*					8514.053*	8540.112	8555.639
15		8464.919*						8539.560)*	8555.959)
								39.365)	56.162)
16		8464.919*	8477.084					8538.798	8556.449*
17		8464.855	8477.814*				8514.250*	8537.999	8556.724
18		8464.613	8478.389*					8537.192	8556.993
19		8464.292*	8479.046*				8514.053*	8536.370	8557.238
20		8463.840	8479.541*		8475.833*		8513.980*	8535.543	8557.439*
21	8434.525*	8463.421*	8479.963*		8475.026	8490.470*	8513.865	8534.672	8557.641
22	8432.863*	8462.815*	8480.331*		8474.157	8489.268*	8513.712	8533.786	8557.804*
23	8431.115	8462.084*	8480.658*		8473.223*	8487.849*	8513.413	8532.876	8557.954*
24	8429.321*	8461.374*	8480.859*		8472.214	8486.513*	8513.122	8531.937	8558.079*
25	8427.481*	8460.532*	8481.059*		8471.153	8485.040	8512.779	8530.988	8558.191*
26	8425.521	8459.660*	8481.167*		8470.004	8483.568	8512.406	8529.946	8558.245*
27	8423.567	8458.726*	8481.167*		8468.819	8482.041	8511.969	8528.969	8558.245*
28	8421.507	8457.703*	8481.167*	8433.667*	8467.559	8480.446	8511.447*	8527.933	8558.245*
29	8419.354*	8456.629	8481.059*	8431.333*	8466.220	8478.824	8510.936*	8526.799	8558.245*
30	8417.136	8455.449	8480.859*	8429.051	8464.855	8477.152	8510.384	8525.732	8558.191*
31	8414.913*	8454.250	8480.658*	8426.561*	8463.421*	8475.437		8524.611*	8558.079*
32	8412.544	8452.951*	8480.331*	8424.102	8461.918*	8473.668	8509.075	8523.419	8557.945*
33		8451.563	8479.936*	8421.635	8460.353	8471.847*	8508.329	8522.211*	8557.724
34	8407.787	8450.131	8479.541*	8419.000	8458.726*	8470.004*	8507.557	8520.976*	
35	8405.228*	8448.638	8479.046*	8416.433	8457.053	8468.075	8506.725		
36	8402.670*	8447.049	8478.540	8413.759*	8455.312	8466.112	8505.850		
37	8399.992	8445.450	8477.896	8410.979	8453.513	8464.098	8504.909		
38	8397.276*	8443.744	8477.229	8408.184	8451.675	8462.034	8503.915*		
39	8394.513	8441.988		8405.313	8449.673	8459.929	8502.894		
40	8391.710	8440.163	8475.677	8402.448*	8447.776	8457.779	8501.811		
41	8388.844*	8438.273	8474.812	8399.438	8445.734*	8455.565	8500.665		
42	8385.855	8436.320	8473.879	8396.420	8443.656	8453.326	8499.478		
43	8382.857	8434.312		8393.343	8441.510	8451.014	8498.230		
44	8379.777	8432.241		8390.246*	8439.315	8448.638*	8496.933		
45	8376.656	8430.107		8387.006	8437.062	8446.261	8495.604		
46	8373.467	8427.908		8383.782	8434.750	8443.806*	8494.171		
47	8370.208*	8425.658		8380.458	8432.390	8441.306*	8492.729		
48	8366.915	8423.336		8377.098	8429.956	8438.748	8491.237		
49	8363.533	8420.961		8373.671	8427.481	8436.145	8489.672		
50		8418.516			8424.948	8433.486	8488.069		
51		8416.033			8422.356	8430.781			
52		8413.479			8419.694	8428.033*			
53		8410.854			8417.016	8425.215			
54		8408.184			8414.253	8422.356			
55		8405.466			8411.454	8419.444			
56		8402.670*			8408.579				
57		8399.819			8405.669				
58		8396.900			8402.670*				
59		8393.945			8399.654				
60		8390.943			8396.560				
61		8387.855			8393.442				

(CONTINUED)

N	Q1	Q2
62	8384.722*	8390.246*
63	8381.622	8387.006
64	8378.287	8383.782
65	8374.797	8380.458
66	8371.622	8377.098*

ACKNOWLEDGMENTS

The capable experimental assistance and friendly hospitality of Mr. Rob Hubbard of the KPNO staff are gratefully acknowledged. Financial support was provided by the Natural Sciences and Engineering Research Council of Canada. We are grateful to Dr. J. K. G. Watson for sending us a copy of his work on the energy levels of $^4\Pi$ states.

RECEIVED: October 23, 1981

REFERENCES

1. H. SPINRAD AND R. F. WING, *Ann. Rev. Astron. Astrophys.* **7,** 249–302 (1969).
2. G. P. KUIPER, W. WILSON, AND R. J. CASHMAN, *Ap. J.* **106,** 243–250 (1947).
3. J. J. NASSAU, G. B. VAN ALLEDA, AND P. C. KEENAN, *Ap. J.* **109,** 333–336 (1949).
4. A. LAGERQVIST AND L-E. SELIN, *Ark. Fys.* **11,** 429–430 (1957).
5. P. C. KEENAN AND L. W. SCHROEDER, *Ap. J.* **115,** 82–88 (1952).
6. A. BUDÓ AND I. KOVÁCS, *Phys. Z.* **45,** 122–126 (1944).
7. I. KOVÁCS "Rotational Structure in the Spectra of Diatomic Molecules," Adam Hilger Ltd., London, 1969.
8. L. VESETH, *Phys. Scr.* **12,** 125–128 (1975).
9. J-L. FÉMÉNIAS, *Canad. J. Phys.* **55,** 1733–1774 (1977).
10. D. L. ALBRITTON, A. L. SCHMELTEKOPF, W. J. HARROP, R. N. ZARE, AND J. CZARNY, *J. Mol. Spectrosc.* **67,** 157–184 (1977); P. C. COSBY, J-B. OZENNE, J. T. MOSELEY, AND D. L. ALBRITTON, *J. Mol. Spectrosc.* **79,** 203–235 (1980); A. CARRINGTON, P. G. ROBERTS, AND P. J. SARRE, *Mol. Phys.* **35,** 1523–1535 (1978).
11. J. M. BROWN AND A. J. MERER, *J. Mol. Spectrosc.* **74,** 488–494 (1979).
12. P. L. RADLOFF AND P. A. FREEDMAN, *Mol. Phys.* **37,** 1633–1638 (1979); P. A. FREEDMAN AND P. L. RADLOFF, *J. Mol. Spectrosc.* **88,** 225–227 (1981).
13. A. BUDÓ, *Z. Phys.* **105,** 73–80 (1937).
14. J. T. HOUGEN, *Canad. J. Phys.* **40,** 598–606 (1962).
15. R. W. MARTIN AND A. J. MERER, *Canad. J. Phys.* **51,** 634–643 (1973).
16. J. M. BROWN AND D. J. MILTON, *Mol. Phys.* **31,** 409–422 (1976).
17. A. S-C. CHEUNG, R. C. HANSEN, AND A. J. MERER, *J. Mol. Spectrosc.* **91,** 165–208 (1982).
18. J. H. VAN VLECK, *Phys. Rev.* **23,** 213–227 (1951).
19. J. M. BROWN, E. A. COLBOURN, J. K. G. WATSON, AND F. D. WAYNE, *J. Mol. Spectrosc.* **74,** 294–318 (1979).
20. D. RICHARDS AND R. F. BARROW, *Nature (London)* **219,** 1244–1245 (1968).
21. L. VESETH, *J. Mol. Spectrosc.* **38,** 228–242 (1971).
22. W. H. HOCKING, A. J. MERER, D. J. MILTON, W. E. JONES, AND G. KRISHNAMURTY, *Canad. J. Phys.* **58,** 516–533 (1980).
23. J. M. BROWN, private communication; J. M. BROWN, D. J. MILTON, J. K. G. WATSON, R. N. ZARE, D. L. ALBRITTON, M. HORANI, AND J. ROSTAS, *J. Mol. Spectrosc.* **90,** 139–151 (1981).
24. R. A. FROSCH AND H. M. FOLEY, *Phys. Rev.* **88,** 1337–1349 (1952); G. C. DOUSMANIS, *Phys. Rev.* **97,** 967–970 (1955).
25. A. CARRINGTON, P. N. DYER, AND D. H. LEVY, *J. Chem. Phys.* **47,** 1756–1763 (1967); J. M. BROWN, I. KOPP, C. MALMBERG, AND B. RYDH, *Phys. Scr.* **17,** 55–67 (1978); C. H. TOWNES AND A. L. SCHAWLOW "Microwave Spectroscopy," McGraw-Hill, New York, 1955.
26. I. C. BOWATER, J. M. BROWN, AND A. CARRINGTON, *Proc. R. Soc. London Ser. A* **333,** 265–288 (1973).